Effects of Sulforaphane on SARS-CoV-2 infection and NF-κB dependent expression of genes involved in the COVID-19 'cytokine storm'

JESSICA GASPARELLO[1], GIOVANNI MARZARO[2], CHIARA PAPI[1], VALENTINA GENTILI[3], ROBERTA RIZZO[3], MATTEO ZURLO[1], CHIARA SCAPOLI[1], ALESSIA FINOTTI[1] and ROBERTO GAMBARI[1]

[1]Department of Life Sciences and Biotechnology, University of Ferrara, I-44121 Ferrara;
[2]Department of Pharmaceutical and Pharmacological Sciences, University of Padova, I-35131 Padova;
[3]Department of Chemical and Pharmaceutical Sciences, University of Ferrara, I-44121 Ferrara, Italy

Received December 30, 2022; Accepted June 9, 2023

DOI: 10.3892/ijmm.2023.5279

Abstract. Since its spread at the beginning of 2020, the coronavirus disease 2019 (COVID-19) pandemic represents one of the major health problems. Despite the approval, testing, and worldwide distribution of anti-severe acute respiratory syndrome coronavirus 2 (SARS-CoV-2) vaccines, the development of specific antiviral agents targeting the SARS-CoV-2 life cycle with high efficiency, and/or interfering with the associated 'cytokine storm', is highly required. A recent study, conducted by the authors' group indicated that sulforaphane (SFN) inhibits the expression of IL-6 and IL-8 genes induced by the treatment of IB3-1 bronchial cells with a recombinant spike protein of SARS-CoV-2. In the present study, the ability of SFN to inhibit SARS-CoV-2 replication and the expression of pro-inflammatory genes encoding proteins of the COVID-19 'cytokine storm' was evaluated. SARS-CoV-2 replication was assessed in bronchial epithelial Calu-3 cells. Moreover, SARS-CoV-2 replication and expression of pro-inflammatory genes was evaluated by reverse transcription quantitative droplet digital PCR. The effects on the expression levels of NF-κB were assessed by western blotting. Molecular dynamics simulations of NF-kB/SFN interactions were conducted with Gromacs 2021.1 software under the Martini 2 CG force field. Computational studies indicated that i) SFN was stably bound with the NF-κB monomer; ii) a ternary NF-kB/SFN/DNA complex was formed; iii) the SFN interacted with both the protein and the nucleic acid molecules modifying the binding mode of the latter, and impairing the full interaction between the NF-κB protein and the DNA molecule. This finally stabilized the inactive complex. Molecular studies demonstrated that SFN i) inhibits the SARS-CoV-2 replication in infected Calu-3 cells, decreasing the production of the N-protein coding RNA sequences, ii) decreased NF-κB content in SARS-CoV-2 infected cells and inhibited the expression of NF-kB-dependent IL-1β and IL-8 gene expression. The data obtained in the present study demonstrated inhibitory effects of SFN on the SARS-CoV-2 life cycle and on the expression levels of the pro-inflammatory genes, sustaining the possible use of SFN in the management of patients with COVID-19.

Correspondence to: Professor Roberto Gambari or Professor Alessia Finotti, Department of Life Sciences and Biotechnology, University of Ferrara, 46 L.Borsari Street, I-44121 Ferrara, Italy
E-mail: gam@unife.it
E-mail: alessia.finotti@unife.it

Abbreviations: SFN, sulforaphane; COVID-19, coronavirus disease 2019; SARS-CoV-2, severe acute respiratory syndrome coronavirus 2; IL, interleukin; RT-qPCR, reverse transcription-quantitative polymerase-chain reaction; NF-kB, nuclear factor-kappa B

Key words: SARS-CoV-2, SFN, NF-kB, pro-inflammatory genes, COVID-19, nutraceuticals

Introduction

Since its spread at the beginning of 2020, the coronavirus disease 2019 (COVID-19) pandemic represents one of the major health problems, causing radical changes in the social behavior of the affected population. Consequently, research efforts have been made to characterize the severe acute respiratory syndrome coronavirus 2 (SARS-CoV-2) sequences and develop novel therapeutic options (1-3). Despite the approval, testing, and worldwide distribution of anti-SARS-CoV-2 vaccines, the COVID-19 pandemic still represents one of the most important challenges in developing specific antiviral agents targeting the SARS-CoV-2 life cycle with high efficiency (4-9). Despite the majority of individuals show moderate symptoms, certain patients develop severe disease, which is generally associated with clinical and laboratory signs of inflammation (10-13). From a molecular point of view, SARS-CoV-2 entry within the cells is mediated by the interaction between the viral surface spike protein and the host cells angiotensin-converting enzyme receptor (14-16). Following its entry into the respiratory epithelial cells, SARS-CoV-2 causes an immune response with inflammatory cytokine production, followed by infiltration of macrophages and

neutrophils into the lung tissue, which results in the cytokine storm (17-20). SARS-CoV-2 activates T lymphocytes, which in turn secrete proinflammatory cytokines, including granulocyte-macrophage colony-stimulating factor and IL-6 (21,22). The cytokine storm in COVID-19 was proposed to occur due to SARS-CoV-2-mediated activation of transcription factors, such as NF-κB and STAT3, which in turn regulate expression of genes involved in inflammation, including vascular endothelial growth factor, monocyte chemoattractant protein 1, IL-8 and IL-6 (23-26).

Among the large variety of pharmaceutical strategies, an increasing number of studies have focused on repurposed drugs and bioactive molecules from natural sources. The isothiocyanate sulforaphane (SFN) is one of the most abundant bioactive components of *Brassicaceae* plants (for example, broccoli) (27,28). SFN is derived from the hydrolysis of its biogenic precursor glucoraphanin, which is mediated by myrosinase. Myrosinases are present not only in plants but also in gastrointestinal microflora; for this reason, they can be administered directly in their active forms or as glucoraphanin (29). As already and extensively reported in previous studies, SFN exhibits a wide range of biological effects including anticancer (30), antioxidant (31), antimicrobial (32), neuroprotective (33), cardioprotective (34), and anti-inflammatory (35) activities. As demonstrated by several studies, the anti-inflammatory activity of SFN is mediated by NF-κB inhibition (36-38). Following its translocation to the nucleus, NF-κB is able to induce the expression of proinflammatory cytokines (39) including, but not limited to IL-6 (40,41), IL-8 (42) and IL-1β (39). It is interesting to note that the results from several phase I and II clinical trials investigating the safety and tolerability of SFN are currently available (43-46).

Recently, it was reported that SFN inhibited the expression of IL-6 and IL-8 genes induced by the treatment of IB3-1 bronchial cells with a recombinant spike protein of SARS-CoV-2 (47). The data reported were in full agreement with the results published by Ordonez *et al* (48) in which SFN was able to inhibit the *in vitro* replication of six SARS-CoV-2 strains, including delta and omicron. In the present study, the ability of SFN to inhibit SARS-CoV-2 replication in SARS-CoV-2 infected Calu-3 cells was investigated along with its effects on the expression levels of NF-κB induced pro-inflammatory genes.

Materials and methods

Cellular models. Experiments were conducted in epithelial respiratory model: Calu-3 cells (cat. no. HTB-55; American Type Culture Collection; cell passage: 36 when they were purchased), isolated from 25-year-old Caucasian man with lung adenocarcinoma (49,50). Cells were cultured in a humidified atmosphere of 5% CO_2 in DMEM/F12 medium (Gibco; Thermo Fisher Scientific, Inc.) supplemented with 10% fetal bovine serum (Biowest), 100 units/ml penicillin, 100 µg/ml streptomycin (Lonza Group, Ltd.), and 1% NEEA (100X) (Non-Essential Amino Acids Solution; Gibco; Thermo Fisher Scientific, Inc.). The number of cells to be seeded was determined using a Z2 Coulter Counter (Beckman Coulter, Inc.).

Chemical compounds. Stock solutions of SFN (D,L-Sulforaphane; cat. no. 574215-25MG; MilliporeSigma) were prepared at final concentration of 150 mM in DMSO (cat. no. D8418; MilliporeSigma). Aliquots of stock solution were prepared and stored at -20˚C (protected from light). Each stock solution of SFN was diluted 1:10 in DMSO just before cell treatment (51,52). Control cell populations cultured in the presence of only DMSO were accordingly employed. The concentration of DMSO in the control population was always identical to that used for the SFN treatment [maximum DMSO concentration used 0.1% (v/v)].

Infection of Calu-3 cells with SARS-CoV-2. SARS-CoV-2 manipulation was performed in the BSL-3 laboratory following the biosafety requirements. SARS-CoV-2 was isolated from a nasopharyngeal swab retrieved from a patient with COVID-19 (Caucasian man of Italian origin, genome sequences available at GenBank (SARS-CoV-2-UNIBS-AP66:ERR4145453, https://trace.ncbi.nlm.nih.gov/Traces/?view=run_browser&acc=ERR4145453&display=metadata). This SARS-CoV-2 isolate clustered in the B1 clade which includes most of the Italian sequences, together with sequences derived from other European countries and USA. The susceptibility of Calu-3 cells to SARS-CoV-2 infection was assayed by infecting single type cell with a MOI of 0.1 for 2 h at 37˚C (~$2x10^5$ infectious virus particles per well, containing 10^6 cells). A total of 24 and 48 h after infection, the infected/treated cells were collected. Viral load within Calu-3 cells was detected 24 and 48 h post-infection (hpi) by reverse transcription-droplet-digital (RT-dd) PCR using SARS-CoV-2 RUO qPCR Primer & Probe kit, according to the manufacturer's instructions (Integrated DNA Technologies, Inc.) which detects two sequences in SARS-CoV-2 N region (N1 and N2) and uses the human RNAse P as a normalizer. Number of copies of SARS-CoV-2 are in the order of 10^9 copies/µg of isolated RNA.

Cellular RNA extraction. Calu-3 SARS-CoV-2-infected cells were lysed in TRI Reagent® (cat. no. T9424; MilliporeSigma) according to the manufacturer's instructions. Obtained RNA pellets were washed with 1 ml of 75% ethanol and centrifuged at 12,000 x g for 5 min at 4˚C. Finally, the pellets were suspended in RNAse-free water and checked for RNA integrity on 1% agarose gel, employing FluoroVue Nucleic Acid Stain as intercalating agent and following the manufacturer's instructions (SMOBIO Technology, Inc.; cat. no. NS1000).

Viral RNA isolation and analysis. RNA was extracted from clarified cell culture supernatants 24 and 48 hpi using PureLink Viral RNA/DNA Mini kit (cat. no. 1228050; Thermo Fisher Scientific, Inc.) according to the manufacturer's instructions. SARS-CoV-2 quantification was performed using the PowerUp SYBR Green Master Mix (Thermo Fisher Scientific, Inc.) targeting the S gene using the following primers: RBD-q forward, 5'-CAATGGTTTAACAGGCACAGG-3' and reverse, 5'-CTCAAGTGTCTGTGGATCACG-3' (Integrated DNA Technologies, Inc.) (53). The standard curve was obtained by determination of copy numbers derived from serial dilutions (10^2-10^8 copies) of the corresponding gene block (Integrated DNA Technologies, Inc.).

Table I. Complete list of employed TaqMan PCR assays.

Target	Assay ID	Sequence
IL-1β	Hs.PT.58.1518186	Purchased from Integrated DNA Technologies, Inc.
IL-6	Hs.PT.58.40226675	Purchased from Integrated DNA Technologies, Inc.
IL-8	Hs.PT.58.38869678.g	Purchased from Integrated DNA Technologies, Inc.
NF-kB p65	Hs.PT.58.22880470	Purchased from Integrated DNA Technologies, Inc.
NF-kB p50	Hs.PT.58.38905484	Purchased from Integrated DNA Technologies, Inc.
β-Actin	Home-made assay	Forward Primer: ACGATGGAGGGGAAGACG Reverse Primer: ACAGAGCCTCGCCTTTG Probe: CCTTGCACATGCCGGAGC
RPL13A	Home-made assay	Forward Primer: GGCAATTTCTACAGAAACAAGTTG Reverse Primer: GTTTTGTGGGGCAGCATACC Probe: CGCACGGTCCGCCAGAAGAT
GAPDH	Home-made assay	Forward Primer: ACATCGCTCAGACACCATG Reverse Primer: TGTAGTTGAGGTCAATGAAGGG Probe: AAGGTCGGAGTCAACGGATTTGGTC
N1-SARS-CoV-2 Protein	SARS-CoV-2 Research Use Only Primer and Probe Sets	Forward Primer: GACCCCAAAATCAGCGAAAT Reverse Primer: TCTGGTTACTGCCAGTTGAATCTG Probe: ACCCCGCATTACGTTTGGTGGACC
N2-SARS-CoV-2 Protein	SARS-CoV-2 Research Use Only Primer and Probe Sets	Forward Primer: TTACAAACATTGGCCGCAAA Reverse Primer: GCGCGACATTCCGAAGAA Probe: CAATTTGCCCCCAGCGCTTCA
RNAse P	SARS-CoV-2 Research Use Only Primer and Probe Sets	Forward Primer: AGATTTGGACCTGCGAGCG Reverse Primer: GAGCGGCTGTCTCCACAAGT Probe: TTCTGACCTGAAGGCTCTGCGCG

SARS-CoV-2, severe acute respiratory syndrome coronavirus 2.

Viral load determination in Calu-3 infected cells. Viral load within Calu-3 cells was detected 24 and 48 hpi by RT-dd PCR using SARS-CoV-2 RUO qPCR Primer & Probe kit (Integrated DNA Technologies, Inc.) which detects two sequences in SARS-CoV-2 N region and in the human RNAse P as normalizer (sequences are reported in Table I). Number of copies of SARS-CoV-2 are in the order of 10^9 copies/μg of isolated RNA.

Reverse transcription-quantitative (RT-q) PCR analysis. For the synthesis of cDNA, a combination of both random hexamers and oligo dT (TaqMan Reverse Transcription Reagents; Thermo Fisher Scientific, Inc.) and 500 ng of total RNA were used. RT-qPCR assay was carried out using gene-specific double fluorescently labelled probes in a CFX96 Touch Real-Time PCR Detection System (Bio-Rad Laboratories, Inc.). Relative expression was calculated using the comparative cycle threshold method ($2^{-\Delta\Delta Cq}$ method) (54) and the endogenous control human β-actin was used as normalizer. Sequences of the employed TaqMan Real Time PCR assay are reported in Table I and more detailed information about the assays are available at: https://eu.idtdna.com/site/order/qpcr/predesignedassay.

Western blotting. For NF-κB (p105/p50 and p65) protein quantification, 20 micrograms of total protein extract (quantified by the BCA method employing Pierce BCA Protein Assay Kit; cat. no. 23225; Thermo Fisher Scientific, Inc.) were denatured for 5 min at 98˚C and loaded on SDS polyacrylamide (8%) gel in Tris-glycine buffer (25 mM Tris, 192 mM glycine, 0.1% SDS). The electro-transfer to 0.2-μm nitrocellulose membrane was performed overnight at 360 mA and 4˚C in electro-transfer with CAPS buffer (25 mM Tris, 192 mM glycine, CAPS 10 mM, 10% methanol). Obtained membranes were stained in Ponceau S solution (MilliporeSigma) to verify protein transfer and incubated in 25 ml of blocking buffer for 1 h at room temperature. After three washes in TBST 1X (0.1% Tween-20), membranes were incubated overnight at 4˚C in primary antibody (complete list of employed antibodies and catalogue number are reported in Table II). The following day, membranes were washed in TBST 1X and incubated for 1 h at room temperature, with an appropriate horseradish peroxidase-conjugated secondary antibody (anti-rabbit IgG HRP-conjugated; 1:2,000; cat no. 7074P3; Cell Signaling Technology, Inc.). The primary antibody against β-actin (cat. no. 4970S; Cell Signaling Technology, Inc.) was used as normalization control (1:1,000 dilution). Nitrocellulose membrane was incubated with 5 ml LumiGLO® detection working solution (cat. no. 7003; Cell Signalling Technology, Inc.) and exposed to x-ray film (Hyperfilm™; cat. no. 28906836; Cytiva). The original uncropped western blotting gels and the relative representative Ponceau S staining of the membranes are shown in Figs. S1, S2, S4 and S5 (uncropped gels) and

Table II. Complete list of employed antibodies in western blot analysis.

Antibody name	Cat. no.	Clonality	Supplier
NF-kB p65 Ab	GTX102090	Rabbit polyclonal	GeneTex, Inc.
NF-kB p105/p50 Ab	GTX133711	Rabbit polyclonal	GeneTex, Inc.
β-actin Ab	4970S	Rabbit polyclonal	Cell Signaling Technology, Inc.

Figs. S3 and S6 (Ponceau staining). Images of the blots were acquired and analyzed using Bio-Rad Image Lab Software v.6.1 (Bio-Rad Laboratories, Inc.).

IL-6 protein quantification by ELISA. Cell supernatants collected from Calu-3 cells infected or not infected with SARS-CoV-2 were collected 24 and 48 h after the infection. IL-6 released into cell culture supernatants was measured by ELISA (cat. no. ab46027; Abcam) following the manufacturer's protocol. Samples were subsequently analyzed on a Sunrise microplate reader (Tecan Group, Ltd.).

Computational studies. All the computational methodologies were carried out on a 32 Core AMD Ryzen 9 3905X, 3.5 GHz Linux Workstation (O.S. Ubuntu 20.04) equipped with GPU (Nvidia Quadro RTX 4000, 8 GB). The 3D structure of NF-κB was obtained from the Protein Data Bank (PDB code: 1NFK), and the structure of SFN was prepared starting from its SMILES code with SeeSAR 12.1.0 software [SeeSAR version 12.1.0; BioSolveIT GmbH, 2022, www.biosolveit.de/SeeSAR]. The docking simulation was performed with SeeSAR 12.1.0 software considering only the protein chain A. Binding sites were identified through the 'find unoccupied binding pockets' option in SeeSAR. A total of 50 independent poses were generated with the default parameters.

Molecular dynamics (MD) simulations were conducted with the Gromacs 2021.1 software (55,56) under the Martini 2 CG force field. CG parametrization of NF-κB and DNA were obtained with martinize2 tool [http://cgmartini.nl/index.php/tools2/proteins-and-bilayers/204-martinize], setting the martini22 as force field and the activating the 'elastic' option for both the protein and the DNA. Protein chains were not merged. CG parametrization of SFN and *n*-nonane were obtained through the automartini tool (57,58). All the CG systems were subjected to: *in vacuo* energy minimization for at most 500 steps; solvation with CG-water (W) containing the 10% of CG-antifreeze water (WF); neutralization with the appropriate number of CG-chlorine ions (CL-); energy minimization for at most 10,000 steps; NVT equilibration with position restraints for 10 nanosec and dt=0.01 ps; NVT equilibration with position restraints for 10 nanosec and dt=0.02 ps; NPT equilibration with position restraints for 50 nanosec and dt=0.02 ps. Production MDs were run for 100 nanosec with dt=0.02 ps at T=300˚K. Barostat, thermostat and the other MD parameters were set according to the general indications reported for the Martini CG force field. Distances and RMSD were obtained using the 'gmx distance' and 'gmx rms' tools in Gromacs (57,58).

Statistical analysis. All the data were normally distributed and presented as the mean ± S.D. Comparison of NF-κB (p105/p50 and p65), IL-1β, IL-6 and IL-8 expression levels between SARS-Cov-2-infected Calu-3 cells and SFN-treated cells was performed using paired Student's t-test. Comparison among intracellular production of SARS-CoV-2 genomes under different treatment conditions, measured after 24 and 48 hpi, was performed using a two-way analysis of variance (ANOVA), followed by Bonferroni's post-hoc tests. For statistical analyses, the STATISTICA version 7.1 software (StatSoft, Inc.) was employed. $P<0.05$ was considered to indicate a statistically significant difference.

Results

Infection of Calu-3 cells with SARS-CoV-2 is associated with upregulation of NF-κB and NF-κB dependent gene expression levels. The susceptibility of Calu-3 cells to SARS-CoV-2 infection was assayed by infecting a single type cell with a MOI of 0.1 for 2 h at 37˚C (~$2x10^5$ infectious viral particles per well, containing 10^6 cells). Following infection, the cells were cultured for 24 and 48 h, and the infected cells were collected following washing in order to remove the cell-free viral particles. For viral RNA detection, RNA extraction was performed 24 and 48 hpi as aforementioned and the viral load within Calu-3 cells was detected at 24 and 48 hpi by RT-ddPCR using SARS-CoV-2 RUO qPCR Primer & Probe kit (Integrated DNA Technologies, Inc.). This method can detect two sequences in the SARS-CoV-2 nucleocapsid (N) protein region (N1 and N2) and uses the human RNAse P as a normalizer. The number of copies of the SARS-CoV-2 were in the order of 10^9 copies/μg of isolated RNA. The data obtained fully supported the conclusion that efficient intracellular replication of SARS-CoV-2 was fully achieved within 24 h (Fig. 1A-C).

The concept that increase in the expression levels of the pro-inflammatory transcription factor NF-κB occurs and is detectable following 24 and 48 h of SARS-CoV-2 infection was supported by the present findings (Fig. 2). This was particularly evident when the analysis was performed on NF-κB p50 mRNA (Fig. 2A) and NF-κBp65 mRNA (Fig. 2B) using RNA isolated from 48-h infected cells. A trend similar to these RT-qPCR data was obtained by performing the western blot experiment (Fig. 2C and D), indicating that the relative content of p105, p50 and p65 NF-κB proteins is increased in SARS-CoV-2 infected cells. The differences in the increased levels found following RT-qPCR and western blotting were expectable, as the sensitivities of these two experimental approaches are different and western blotting, unlike RT-qPCR, is not quantitative. Since the increased

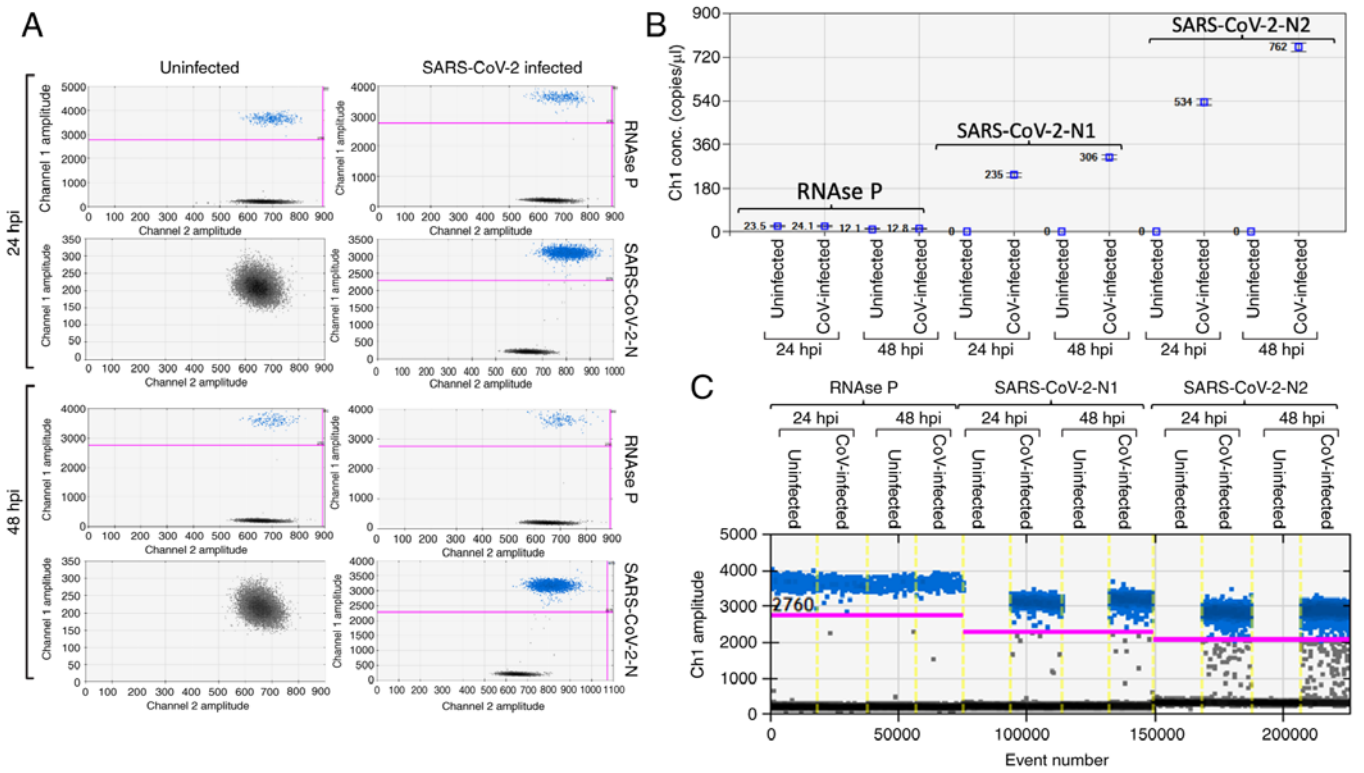

Figure 1. Quantification of SARS-CoV-2 genomes in infected Calu-3 cells. SARS-CoV-2 has been quantified by reverse transcription-digital-droplet PCR. (A) Representative 2D plots obtained by the quantification of human RNAse P and N1-SARS-CoV-2 sequence are reported. (B) Detected copies/μl in each reaction well are reported, for technical issue starting cDNA employed for N1 and N2-SARS-CoV-2 sequences have been diluted 1:10,000 before performing the amplification, while as regard RNAse P 1 μl of starting cDNA has been amplified. (C) Example of 1D plot. SARS-CoV-2, severe acute respiratory syndrome coronavirus 2.

content of the NF-κB mRNAs (Fig. 2A and B) and proteins (Fig. 2C and D) was assessed in SARS-infected Calu-3 cells, the possible effects of SARS-CoV-2 infection were examined on the expression levels of NF-κB regulated genes. The first effects noted on the changes of the transcription factors are expected to involve the contents of the transcripts on the regulated genes. Therefore, the present study focused on examining the expression levels of IL-1β, IL6 and IL-8 mRNAs, which encode for proteins that belong to the so-called 'COVID-19 cytokine storm' (Fig. 3A-D).

The increase in the extracellular release of the protein encoded by the most upregulated gene (IL-6; Fig. 3C) was confirmed by ELISA following quantification of the released IL-6 protein in the supernatants of the SARS-CoV-2-infected cell cultures (Fig. 3D). As expected, the increased release of IL-6 was found, in particular, in Calu-3 cultures exposed for 48 h to SARS-CoV-2. Focus was particularly addressed on IL-6 because the release of this protein has a central role in COVID-19 cytokine storm (13,14). IL-1β, that together with IL-6 plays a major role in the cytokine storm (17) was not considered, since it is released at very low level in Calu3 cells (data not shown).

Binding of SFN to NF-kB: a bioinformatic analysis. One of the possible mechanisms of action of SFN was the inhibition of the activity of certain transcription factors. In this regard, it is well established that SFN induces nuclear factor erythroid 2-related factor. Among possible transcription factors involved in the SARS-CoV-2 life cycle and in the activation of the 'cytokine storm', NF-κB is of relevance, since inhibitors of NF-κB and STAT-3 were found to be particularly effective against SARS-CoV-2. As a first approach, it was assessed by docking-experiments whether SFN can bind to NF-kB. The docking studies were conducted using the software SeeSAR, starting from the crystallographic complex of NF-κB with DNA (PDB-id: 1NFK). The p60 monomer structure was extracted from the complex and the potential binding sites were automatically determined through the 'find unoccupied binding pockets' option in SeeSAR (Fig. 4A). SFN was subsequently docked against all the binding sites, generating 50 poses. A total of 48 poses were generated in the same region, suggesting that the most probable binding site was surrounded by Arg54, Arg56 and His64 (Fig. 4B). The superimposition of the binding pose of SFN with the full 1NFK structure indicated that the compound-protein interaction occurred in the DNA binding region, which impaired the interaction with the nucleic acid. These results are in consistency with the data reported in a previous study demonstrating that SFN inhibits NF-κB binding to DNA and NF-kB-dependent luciferase activity when luc-reporter plasmids were used under the control of NF-κB regulatory promoter regions (52).

To further explore the mechanism of the inhibitory action of SFN on NF-kB, MD studies were conducted. Due to the large dimensions of the system under consideration, the Martini coarse-grained (CG) force field was used. Indeed, CG-MD allows the conduct of long simulations at a reasonable computational cost, while retaining the majority of the chemical information. Indeed, the Martini force field

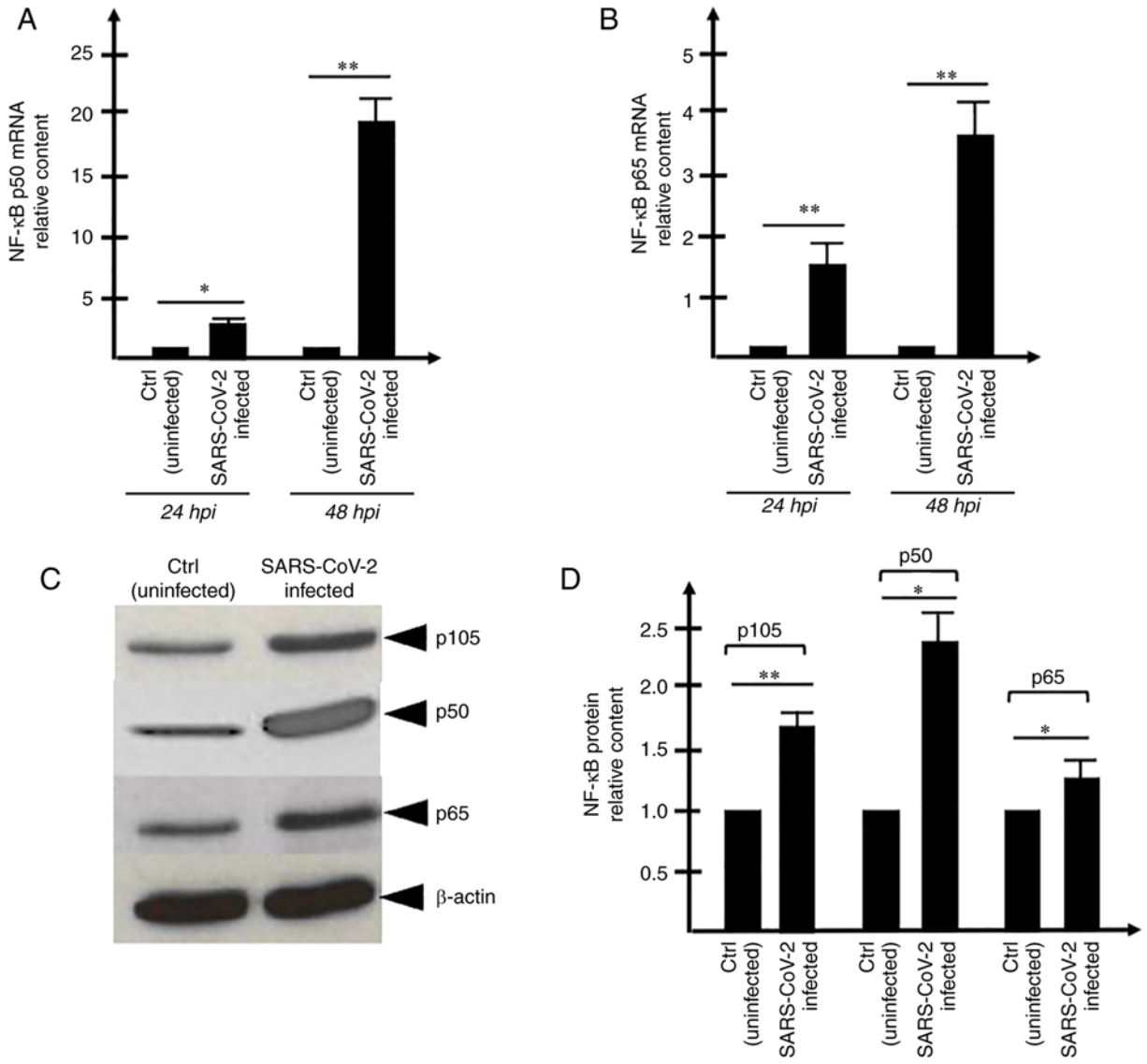

Figure 2. Effects of Calu-3 exposure to SARS-CoV-2. (A and B) Expression of mRNAs coding for (A) NF-κB p50 and (B) NF-κB p65 following 24- and 48-h infection of Calu-3 cells with SARS-CoV-2, as indicated. Results represent the fold increase with respect to uninfected control Calu-3 cells in three independent cultures. (C) Representative example of the western blot data obtained. The membrane was first incubated with an antibody recognizing NF-kB p105/p50, then stripped, washed and incubated with a NF-kB p65 antibody, then stripped, washed and incubated with a control antibody recognizing β-actin. The antibodies used are enlisted in Table II. The original uncut autoradiograms are shown in Figs. S1 and S2. (D) The protein/β-actin ratios obtained after densitometry analysis of the data shown in panel C; ChemiDoc instrument and Image Lab software (both from Bio-Rad Laboratories, Inc.) were used for densitometric analysis of the obtained bands (n=3). The Ponceau staining of the membrane is shown in Fig. S3, confirming the loading quality of the experiment. *P<0.05 and **P<0.01. SARS-CoV-2, severe acute respiratory syndrome coronavirus 2.

has been extensively used to investigate protein-protein as well as ligand-protein interactions, yielding results in great accordance with all-atoms simulations (59-61). In the present study, the Martini 2 force field was used along with the elastic network approach in order to retain the secondary structures of NF-κB and that of the DNA molecule (62).

A preliminary CG-MD simulation was run using the crystallographic complex NF-kB/DNA, measuring the distance between the centers of the mass (com) of the DNA molecule and each chain of the NF-κB protein. The system resulted in a highly stable formulation during the entire simulation time (100 nanosec; Fig. 5A), with the distances com-DNA/com-chain A and com-DNA/com-chain B both fluctuating around the same value (2.23±0.04 nm). Since the molecular docking studies suggested that SFN could bind to the chain A of NF-κB impairing the interaction with the DNA, the chain A was slightly shifted from the nucleic acid, while maintaining the contact with chain B. In this way a putative structure was prepared where the SFN could be accommodated in the complex NF-kB/DNA without any clashes with the DNA. When a CG-MD simulation was run without the SFN, the original NF-kB/DNA complex was restored within ~72 nanosec (Fig. 5B) as demonstrated by the variation of the values of com-DNA/com-chain A (t=0-72 nanosec: 2.38±0.06 nm; t=72-100 nanosec: 2.25±0.03 nm). Conversely, in the presence of SFN, the original complex was not restored during the 100 nanosec of the simulation and the distance com-DNA/com-chain A remained always closed to the displaced value (2.39±0.04 nm), further suggesting that SFN could impair the correct binding of the transcription

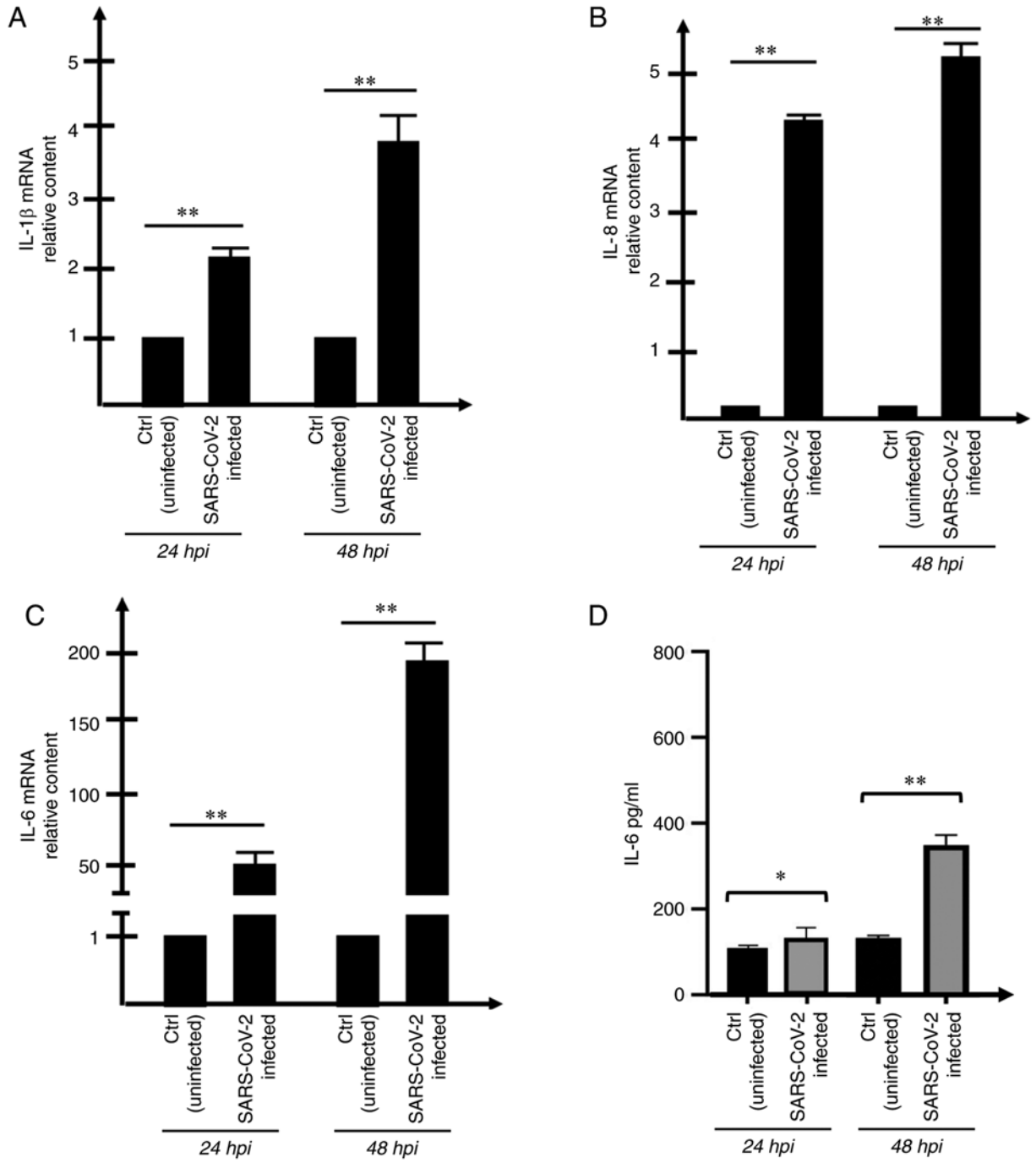

Figure 3. Increased expression of NF-kB-regulated genes in SARS-CoV-2 infected cells. (A-C) Reverse transcription-quantitative PCR analysis was performed using primers/probes detecting (A) IL-1β, (B) IL-8 and (C) IL-6 mRNAs. (D) Quantification of IL-6 content in Calu-3 SARS-CoV-2 infected cells by ELISA test. IL-6 content expressed in pg/ml was determined 48 h after the infection with SARS-CoV-2. *P<0.05 and **P<0.01. SARS-CoV-2, severe acute respiratory syndrome coronavirus 2.

factor with the DNA (Fig. 5C). To exclude that the MD simulation was biased by the simplification introduced by the CG approach, the SFN was replaced with a 'decoy' ligand (namely the *n*-nonane) characterized by the same number of CG particles as that of the SFN but with different features (*i.e.*, the absence of any H-bond acceptor capability and consequently the absence of the binding ability with the protein). As revealed in Fig. 5D, the presence of the nonane (readily displaced from the protein) had no effect on the time required to restore the complex (~72 nanosec; Fig. 5D with Fig. 5B).

The inspection of the ligand root mean square deviation along the trajectory revealed that the SFN changed its position and interactions during the simulation (red curve in Fig. 5E). This displacement was not observed when the CG-MD was run considering only SFN and chain-A (blue curve in Fig. 5E). Accordingly, the following conclusions could be postulated that: i) SFN was stably bound to the NF-κB monomer; ii) a ternary NF-kB/SFN/DNA complex was formed; iii) SFN interacted with both the protein and the nucleic acid modifying its binding mode (Fig. 5F) and impairing the full interaction

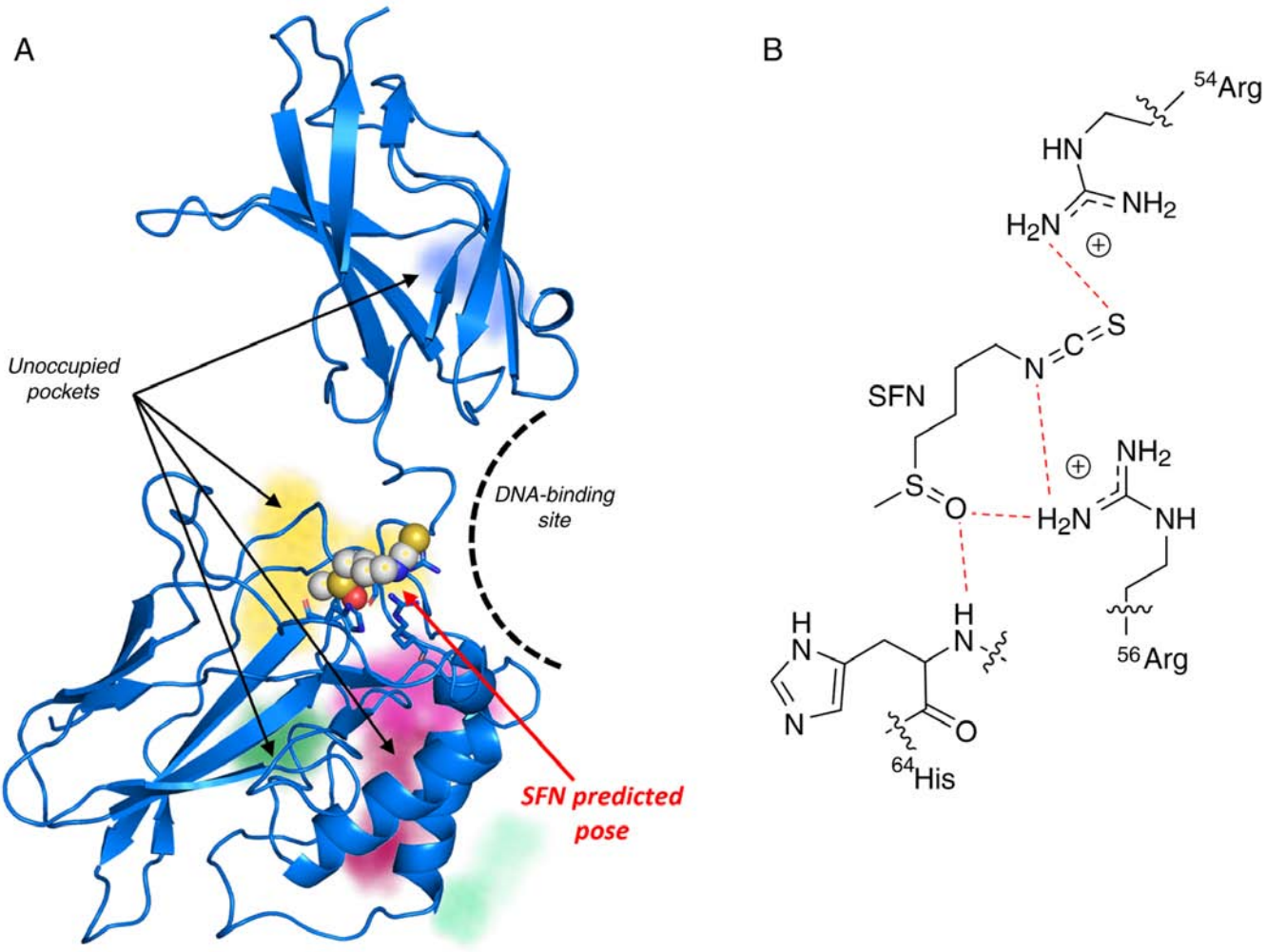

Figure 4. Summary of docking results. Unoccupied pockets (yellow, pink, green and blue transparent surfaces) and predicted binding site for SFN (atom colored spheres) in NF-κB (blue cartoon) as predicted by SeeSAR. (A) Detail of the interaction between NF-κB residues and SFN in the predicted binding site. (B) H-bonds are highlighted as dashed red lines. SFN, sulforaphane.

between the NF-κB and DNA molecules, which finally stabilized the inactive complex.

SFN inhibits SARS-CoV-2 intracellular replication and viral release from infected cells. In order to determine the effects of SFN on SARS-CoV-2 infection, Calu-3 cells were infected with SARS-CoV-2 and the effects of SFN were determined on the extracellular release of SARS-CoV-2 genomes after 24 and 48 hpi and on the intracellular production of SARS-CoV-2 genomes. The results obtained in Calu-3-infected, SFN-treated cells were compared with Calu-3-infected cells cultured in the presence of DMSO (the vehicle of SFN), as DMSO affects both extracellular release and intracellular production of SARS-CoV-2 genomes. As demonstrated in Fig. 6A-C, treatment of the SARS-CoV-2-infected Calu-3 cells with SFN was associated with inhibition of SARS-CoV-2 replication. As expected, the extracellular release of SARS-CoV-2 genomes was significantly higher 48 hpi (Fig. 6A). Moreover, SFN was able to inhibit the extracellular release of SARS-CoV-2 genomes both at 24 and 48 hpi.

This latter conclusion was fully supported by the results obtained studying the intracellular SARS-CoV-2 genome copies detected by RT-ddPCR (representative examples are shown in Fig. 6D and E). In order to quantify the intracellular SARS-CoV-2 content, two assays, which were both able to amplify nucleocapsid protein mRNA, yet in different regions, were employed. The human RNAse P sequence was used as a template loading control. The results obtained demonstrated a decrease of intracellular SARS-CoV-2 genomes following SFN treatment of SARS-CoV-2 infected cells studied 24 and 48 hpi (Fig. 6F and G).

Two-way ANOVA, shown in Fig. S7 and summarized in (Fig. 6F and G), demonstrated a strong significance ($P<0.0001$) of both main effects (24 vs. 48 hpi and different treatments) for both N1 (Fig. S7A) and N2 (Fig. S7B) gene sequences. Specifically, post-hoc comparisons revealed that the difference found when analysing samples at 24 and 48 hpi was highly significant ($P<0.0001$ for both N1 and N2 gene sequences, Fig. S7) considering time, as expected, as a major parameter affecting the total accumulation of intracellular SARS-CoV-2 sequences. In addition, the differences between SFN-treated SARS-CoV-2-infected cells and control DMSO-cultured SARS-CoV-2-infected cells were also found highly significant both at 24 and 48 hpi, considering both N1 (Fig. 6F) and N2 (Fig. 6G) gene sequences.

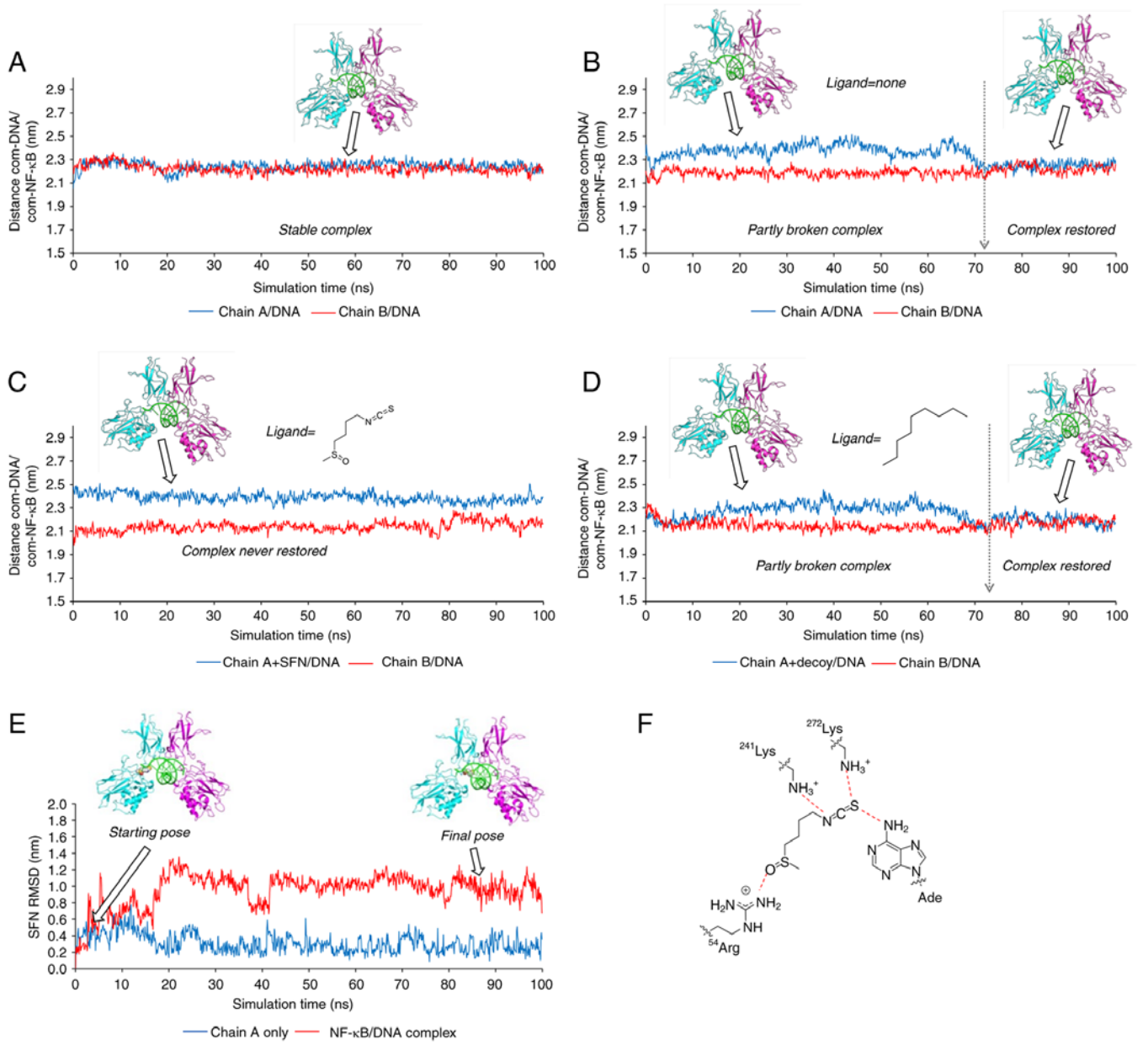

Figure 5. Results from CG-MD simulations. (A) Time-dependent distance between com-DNA and com-chain A (blue) and between com-DNA and com-chain B (red) of the original NF-kB/DNA complex. (B) Time-dependent distance between com-DNA and com-chain A (blue) and between com-DNA and com-chain B (red) of the chain-A displaced NF-kB/DNA complex in the absence of any ligand. (C) Time-dependent distance between com-DNA and com-chain A (blue) and between com-DNA and com-chain B (red) of the chain-A displaced NF-kB/DNA complex in the presence of SFN bound to chain A. (D) Time-dependent distance between com-DNA and com-chain A (blue) and between com-DNA and com-chain B (red) of the chain-A displaced NF-kB/DNA complex in the presence of a decoy ligand (n-nonane) bound to chain A. (E) Time-dependent SFN RMSD (nm) bound to chain A alone (blue) and bound to the entire NF-kB/DNA complex (red). (F) Detail of the interaction between NF-kB/DNA and SFN at the end of the 100 ns of CG-MD simulation. H-bonds are highlighted as dashed red lines. Note that the H-bond with 54Arg was retained along the entire simulation. A video of the CG-MD simulation is also available (Video S1). CG-MD, coarse-grained molecular dynamics; SFN, sulforaphane.

Collectively, the data shown in Fig. 6 demonstrated that SFN inhibited SARS-CoV-2 intracellular replication (Fig. 6F and G) as well as the viral release in the extracellular environment (Fig. 6B and C). Despite the fact that the inhibitory effects were slightly different when the two RT-PCR methods (absolute RT-qPCR and RT-ddPCR) were compared, the results obtained were consistent with the hypothesis stating that SFN inhibits SARS-CoV-2 life cycle.

Expression of NF-κB is downregulated in SARS-CoV-2 infected, SFN-treated Calu-3 cells. Since it has been reported that the SARS-CoV N-protein binds to the NF-κB promoter, thereby stimulating the NF-κB transcription (63), further investigations were conducted to determine whether lower expression of the N-protein gene (Fig. 6F and G) was associated with lower expression of NF-kB. Therefore, the content of NF-κB p50 and p65 mRNA was initially analyzed in SARS-CoV-2-infected, SFN-treated Calu-3 cells (Fig. 7A and B).

The results demonstrated that the contents of NF-κB p50 and p65 mRNA were significantly lower when samples from SARS-CoV-2-infected, SFN-treated Calu-3 cells were compared with samples of SARS-CoV-2-infected

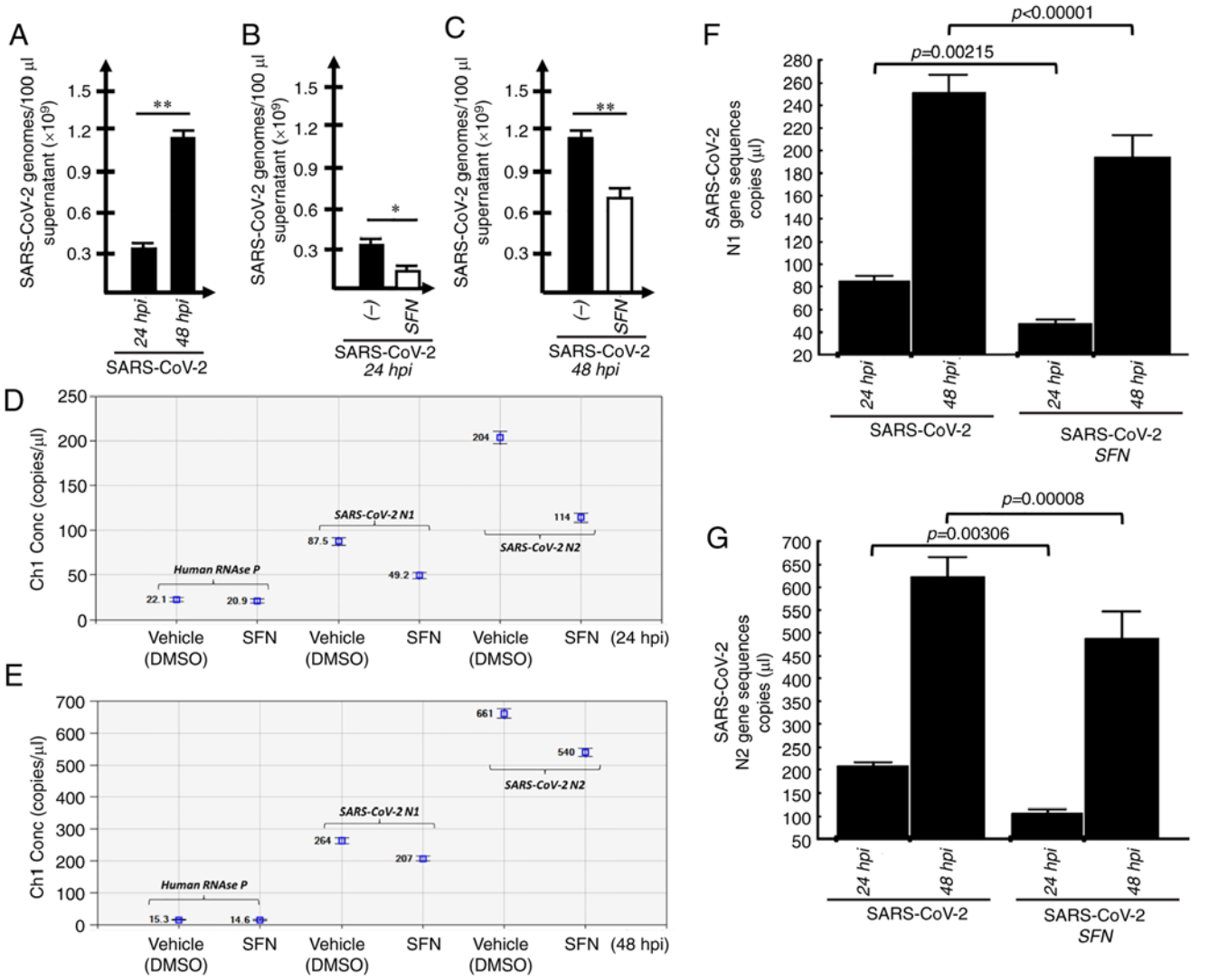

Figure 6. Quantification of SARS-CoV-2 genomes in Calu-3 SARS-Cov-2-infected and SFN-treated cells. (A-C) The amount of SARS-CoV-2-released genomes was determined by absolute reverse transcription-quantitative PCR and compared in (A) Calu-3 infected cells analyzed 24 and 48 hpi, or in Calu-3 infected cells treated with SFN or with the SFN vehicle DMSO and analyzed (B) 24 and (C) 48 hpi (n=3) *P<0.05, significant; **P<0.01, highly significant. (D and E) Representative reverse transcription-digital-droplet dPCR 2D plots quantifying intracellular SARS-CoV-2 genomic N1 and N2 sequences (as indicated); samples were isolated at (D) 24 and (E) 48 hpi time points. (F and G) Two-way ANOVA, followed by post hoc Bonferroni test (see also Fig. S7) performed on samples from SARS-CoV-2-infected Calu-3 cells in the absence or in the presence of SFN, as indicated. Cells were harvested at 24 and 48 hpi. The results represent the mean ± S.D. (n=6). The analysis of the data shown in panels F and G is further detailed in Fig. S7. For SARS-CoV-2 genome quantification, the N1 (F) and N2 (G) sequences have been considered. The P-values reported in panels F and G (two-way ANOVA, followed by post hoc Bonferroni test) were obtained comparing untreated infected cells (SARS-CoV-2) vs. SFN-treated infected cells (SARS-CoV-2 + SFN). Results represent the mean ± S.D. SARS-CoV-2, severe acute respiratory syndrome coronavirus 2; hpi, h post-infection; SFN, sulforaphane.

cells. Western blotting confirmed this trend, as indicated in Fig. 7C and D.

Expression of NF-κBregulated pro-inflammatory genes in SARS-CoV-2-infected, SFN-treated Calu-3 cells. Considering the inhibitory effects on NF-κB (Fig. 7A and B), subsequent studies aimed to determined whether the expression levels of pro-inflammatory genes were modified following treatment of SARS-CoV-2-infected Calu-3 cells with SFN. To this end, the expression levels of the mRNAs encoding IL-1β, IL-6 and IL-8 were assessed by RT-qPCR in SARS-CoV-2 infected, SFN-treated Calu-3 cells (Fig. 8). The results obtained demonstrated that the expression levels of IL-1β (Fig. 8A) and IL-8 (Fig. 8C) were significantly reduced when samples from SARS-CoV-2-infected, SFN-treated Calu-3 cells were compared with samples of SARS-CoV-2-infected cells. It is notable that all these regulatory proteins belong to the 'COVID-19 cytokine storm'. Regarding the expression of IL-6, non-significant changes were detected (Fig. 8B); however, this may be caused by the high activation of this gene following SARS-CoV-2 infection (Fig. 3).

Discussion

In the present study, the effects of SFN were characterized on the bronchial epithelial cell line Calu-3 infected by SARS-CoV-2 with regard to the replication of the viral genome and the possible inhibition of gene encoding pro-inflammatory proteins. The present study is related to previously published observations indicating that SFN was able to inhibit the

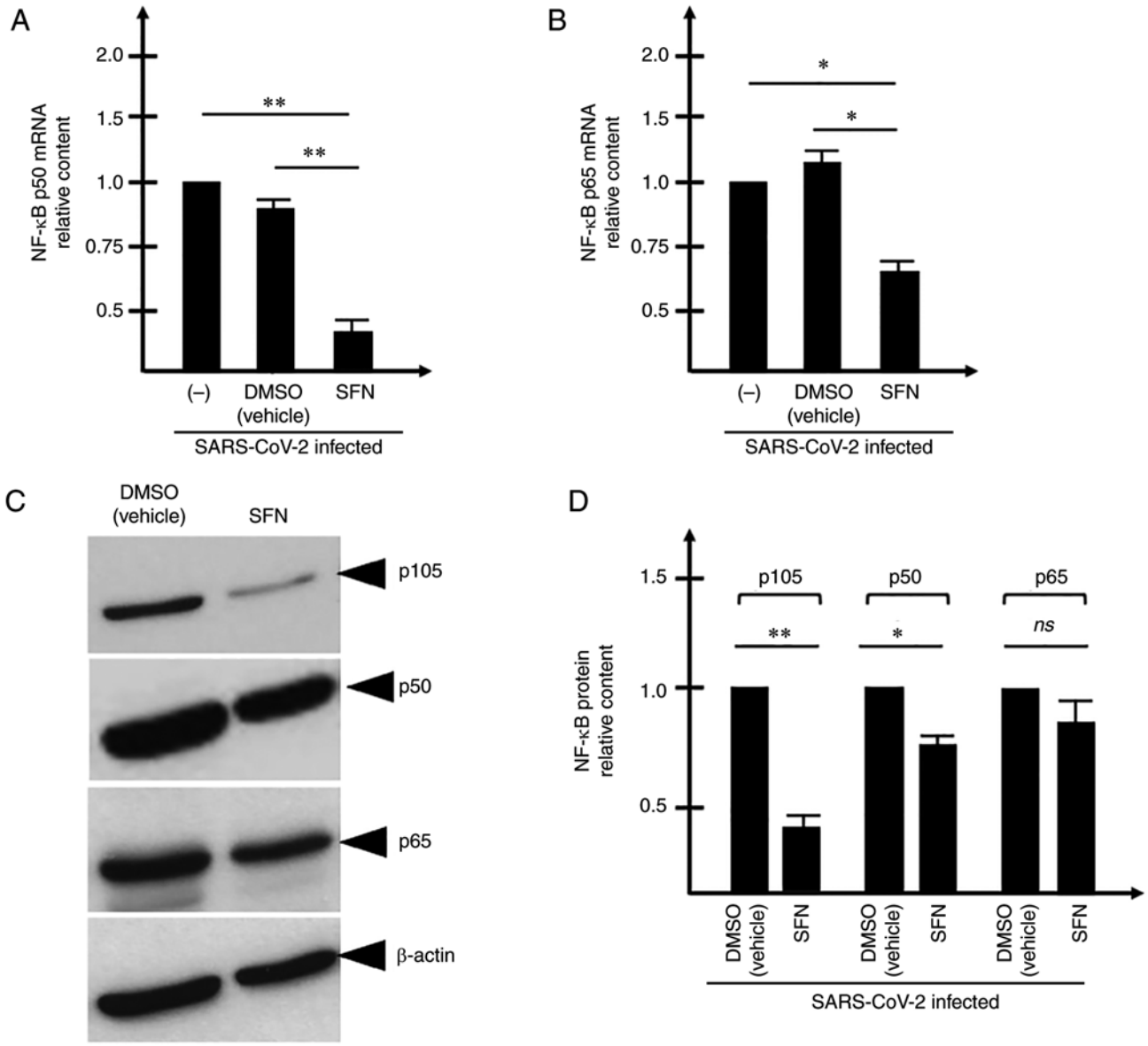

Figure 7. Quantification of NF-κB gene expression in Calu-3 SARS-Cov-2 infected, SFN-treated cells. (A and B) For quantification of NF-κB mRNAs, reverse transcription-quantitative PCR was employed to quantify the expression of transcripts coding for (A) NF-κBp50 subunit and (B) NF-κBp65 subunit. (C and D) NF-κB proteins were quantified by western blotting. (C) Representative Western Blot membranes hybridized with antibodies against NF-κB (p105/50, p65) and b-actin (as endogenous control). The original uncropped gels used for panel C are shown in Figs. S4 and S5. Representative Ponceau S staining of the membranes to verify extracts loading in each sample is presented in Fig. S6. (D) Quantitative analysis of the protein/β-actin ratios obtained after densitometric analysis of the data shown in panel C; ChemiDoc instrument and Image Lab software (both from Bio-Rad Laboratories, Inc.) were used densitometry analysis of the obtained bands (n=3). *P<0.05 and **P<0.01. SARS-CoV-2, severe acute respiratory syndrome coronavirus 2; SFN, sulforaphane.

expression levels of IL-6 and IL-8 genes induced by the treatment of IB3-1 bronchial cells with a recombinant spike protein of SARS-CoV-2 (46).

In the current study, the Calu-3 cellular system was characterized with regard to the SARS-CoV-2-induced increase in the expression levels of NF-κB and NF-κB-regulated pro-inflammatory genes. A highly significant increase in the expression levels of these genes has been demonstrated to be associated with SARS-CoV-2 infection of Calu-3 cells. SFN-mediated inhibition of SARS-CoV-2 replication was analyzed by RT-ddPCR and by RT-qPCR quantification of the release of SARS-CoV-2 genomes by the infected cells. It was found that SFN could inhibit SARS-CoV-2 replication by analyzing either the intracellular amount of N-protein sequences or the release of the virus; this led to the subsequent analysis of the SARS-CoV-2 genomes present in the supernatants of SFN-treated, SARS-CoV-2-infected Calu-3 cells. With the regard to its effects on the pro-inflammatory genes, SFN was able to inhibit upregulation of NF-κB expression in SARS-CoV-2-infected cells. It is worth noting that molecular docking studies suggested a direct interaction of SFN to the DNA binding region of NF-κB. Further MD simulations provided additional information on the potential mechanism of action of SFN at the molecular level, suggesting that this compound could impair the formation of the effective protein/DNA complex (Video S1). The results obtained from the quantification of mRNAs encoding IL-1β, IL-6 and IL-8, indicated that SFN exerted an inhibitory

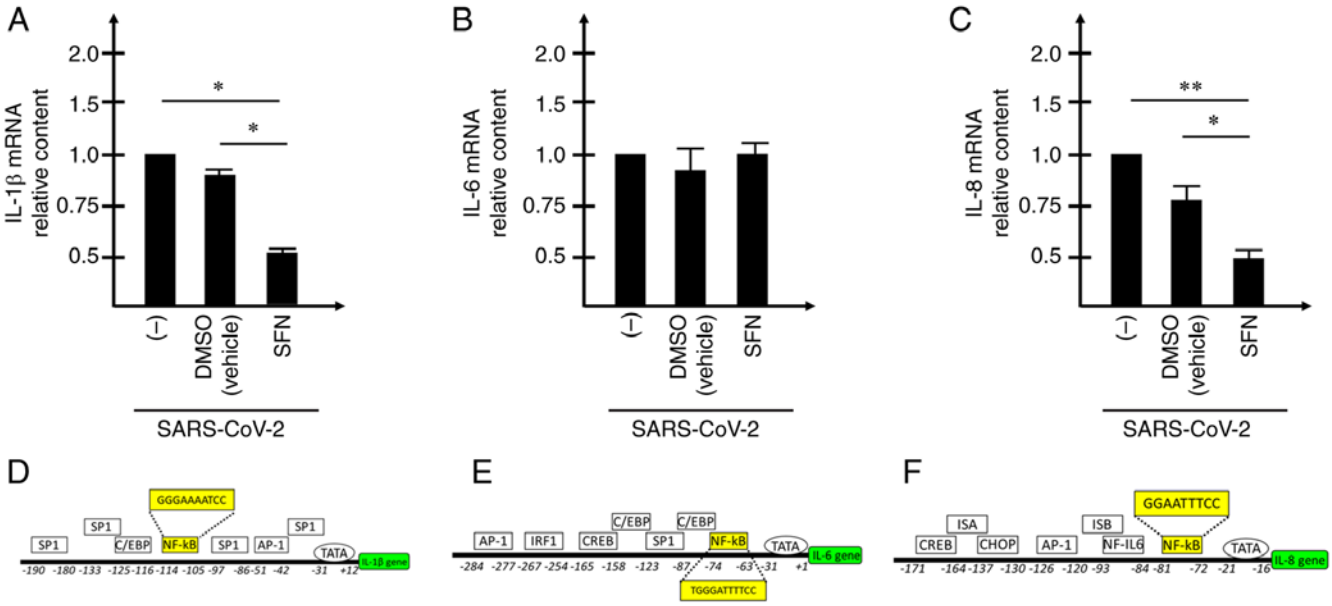

Figure 8. Expression of pro-inflammatory genes in SARS-CoV-2-infected, SFN-treated Calu-3 cells. A short list of pro-inflammatory mRNAs encoding cytokines belonging to the 'COVID-19 cytokine storm' were quantified by reverse transcription-quantitative PCR in SFN-treated Calu-3 cells: (A) IL-1β mRNA, (B) IL-6 mRNA and (C) IL-8 mRNA. (D-F) Binding sites of key transcription factors interacting with the (D) IL-1β, (E) IL-6 and (F) IL-8 gene promoters. *P<0.05 and **P<0.01. SARS-CoV-2, severe acute respiratory syndrome coronavirus 2; SFN, sulforaphane.

effect on IL-1β and IL-8 mRNA levels. The assessment of the SFN effects on IL-6 should be further analyzed, as the downregulation of this pro-inflammatory gene was not detectable under these experimental conditions, possibly due to the very high levels of SARS-CoV-2-mediated induction (>180 fold, when infected cells were compared with uninfected cells).

The data obtained in the present study are in strong agreement with other studies indicating inhibitory effects of SFN on SARS-CoV-2 life cycle (48) and the possible use of this compound in the management of patients with COVID-19 patients, as recently suggested in different studies (64-67).

Based on the evidence, it is important to note that the management of the COVID-19 pandemic requires antiviral agents targeting SARS-CoV-2 life cycle with high efficiency despite the approval, testing, and worldwide distribution of anti-SARS-CoV-2 vaccines (4-8).

The present study contains certain limitations, the most relevant being that only a low number of pro-inflammatory genes were studied in SARS-CoV-2-infected cells. Therefore, the present study should be considered a proof-of-principle study indicating that SFN may be a double-acting agent (a SARS-CoV-2 replication inhibitor and an anti-inflammatory compound).

The analysis of other pro-inflammatory genes involved in the COVID-19 'cytokine storm' should be conducted in order to determine whether the SFN-mediated inhibitory effects noted on the expression levels of IL-1β and IL-8 can be generalized to all the other genes involved in the COVID-19 associated hyper-inflammatory state. This experimental plan will also clarify the relationship between the SFN-mediated effects on genes involved in the COVID-19 'cytokine storm' and the corresponding alterations noted in the regulation of the NF-κB pathway.

Acknowledgements

Not applicable.

Funding

The present study was supported by the MUR-FISR COVID-miRNAPNA Project (grant no. FISR2020IP_04128), the Interuniversity Consortium for Biotechnologies in Italy (grant no. CIB-Unife-2020-1), the CARIPARO Foundation (grant no. MARZ_CARIVARI20_01 C94I20002500007) and the FIRC-AIRC 'Michele e Carlo Ardizzone' fellowship (grant no. 25528).

Availability of data and materials

The datasets used and/or analyzed during the current study are available from the corresponding author on reasonable request.

Authors' contributions

JG, AF, GM, VG and RG curated data. JG, GM, CS, VG, RG and AF performed formal analysis. RG acquired funding. JG, CP, MZ, GM and VG conducted investigation. JG, CP, CS, VG, RR and GM developed methodology. RG, AF, RR, CS, and GM supervised the study. JG, RG, AF, GM, VG and RR wrote the original draft. JG, GM, CP, MZ, VG, RR, CS, RG and AF wrote, reviewed and edited the manuscript. All authors have read and approved the final version of the manuscript. JG, AF and RG confirm the authenticity of all the raw data.

Ethics approval and consent to participate

Not applicable.

Patient consent for publication

Not applicable.

Competing interests

The authors declare that they have no competing interests.

References

1. Walker PGT, Whittaker C, Watson OJ, Baguelin M, Winskill P, Hamlet A, Djafaara BA, Cucunubá Z, Olivera Mesa D, Green W, *et al*: The impact of COVID-19 and strategies for mitigation and suppression in low- and middle-income countries. Science 369: 413-422, 2020.
2. Khan S, Siddique R, Ali A, Bai Q, Li Z, Li H, Shereen MA, Xue M and Nabi G: The spread of novel coronavirus has created an alarming situation worldwide. J Infect Public Health 13: 469-471, 2020.
3. Killerby ME, Biggs HM, Midgley CM, Gerber SI and Watson JT: Middle east respiratory syndrome coronavirus transmission. Emerg Infect Dis 26: 191-198, 2020.
4. Watson OJ, Barnsley G, Toor J, Hogan AB, Winskill P and Ghani AC: Global impact of the first year of COVID-19 vaccination: A mathematical modelling study. Lancet Infect Dis 22: 1293-1302, 2022.
5. Tulimilli SV, Dallavalasa S, Basavaraju CG, Kumar Rao V, Chikkahonnaiah P, Madhunapantula SV and Veeranna RP: Variants of severe acute respiratory syndrome coronavirus 2 (SARS-CoV-2) and vaccine effectiveness. Vaccines (Basel) 10: 1751, 2022.
6. Villamagna AH, Gore SJ, Lewis JS and Doggett JS: The need for antiviral drugs for pandemic coronaviruses from a global health perspective. Front Med (Lausanne) 7: 596587, 2020.
7. Takashita E, Kinoshita N, Yamayoshi S, Sakai-Tagawa Y, Fujisaki S, Ito M, Iwatsuki-Horimoto K, Halfmann P, Watanabe S, Maeda K, *et al*: Efficacy of antiviral agents against the SARS-CoV-2 omicron subvariant BA.2. N Engl J Med 386: 1475-1477, 2022.
8. Kumari M, Lu RM, Li MC, Huang JL, Hsu FF, Ko SH, Ke FY, Su SC, Liang KH, Yuan JP, *et al*: A critical overview of current progress for COVID-19: Development of vaccines, antiviral drugs, and therapeutic antibodies. J Biomed Sci 29: 68, 2022.
9. Zhu C, Lee JY, Woo JZ, Xu L, Nguyenla X, Yamashiro LH, Ji F, Biering SB, Van Dis E, Gonzalez F, *et al*: An intranasal ASO therapeutic targeting SARS-CoV-2. Nat Commun 13: 4503, 2022.
10. Mondal S, Quintili AL, Karamchandani K and Bose S: Thromboembolic disease in COVID-19 patients: A brief narrative review. J Intensive Care 8: 70, 2020.
11. Zong X, Gu Y, Yu H, Li Z and Wang Y: Thrombocytopenia is associated with COVID-19 severity and outcome: An updated meta-analysis of 5637 patients with multiple outcomes. Lab Med 52: 10-15, 2021.
12. Smilowitz NR, Kunichoff D, Garshick M, Shah B, Pillinger M, Hochman JS and Berger JS: C-reactive protein and clinical outcomes in patients with COVID-19. Eur Heart J 42: 2270-2279, 2021.
13. Santa Cruz A, Mendes-Frias A, Oliveira AI, Dias L, Matos AR, Carvalho A, Capela C, Pedrosa J, Castro AG and Silvestre R: Interleukin-6 is a biomarker for the development of fatal severe acute respiratory syndrome coronavirus 2 pneumonia. Front Immunol 12: 613422, 2021.
14. Hu B, Huang S and Yin L: The cytokine storm and COVID-19. J Med Virol 93: 250-256, 2021.
15. Iwasaki M, Saito J, Zhao H, Sakamoto A, Hirota K and Ma D: Inflammation triggered by SARS-CoV-2 and ACE2 augment drives multiple organ failure of severe COVID-19: Molecular mechanisms and implications. Inflammation 44: 13-34, 2021.
16. Yang J, Petitjean SJL, Koehler M, Zhang Q, Dumitru AC, Chen W, Derclaye S, Vincent SP, Soumillion P and Alsteens D: Molecular interaction and inhibition of SARS-CoV-2 binding to the ACE2 receptor. Nat Commun 11: 4541, 2020.
17. Song P, Li W, Xie J, Hou Y and You C: Cytokine storm induced by SARS-CoV-2. Clin Chim Acta 509: 280-287, 2020.
18. Hazeldine J and Lord JM: Neutrophils and COVID-19: Active participants and rational therapeutic targets. Front Immunol 12: 680134, 2021.
19. Veenith T, Martin H, Le Breuilly M, Whitehouse T, Gao-Smith F, Duggal N, Lord JM, Mian R, Sarphie D and Moss P: High generation of reactive oxygen species from neutrophils in patients with severe COVID-19. Sci Rep 12: 10484, 2022.
20. Sefik E, Qu R, Junqueira C, Kaffe E, Mirza H, Zhao J, Brewer JR, Han A, Steach HR, Israelow B, *et al*: Inflammasome activation in infected macrophages drives COVID-19 pathology. Nature 606: 585-593, 2022.
21. Moss P: The T cell immune response against SARS-CoV-2. Nat Immunol 23: 186-193, 2022.
22. Mohammed RN, Tamjidifar R, Rahman HS, Adili A, Ghoreishizadeh S, Saeedi H, Thangavelu L, Shomali N, Aslaminabad R, Marofi F, *et al*: A comprehensive review about immune responses and exhaustion during coronavirus disease (COVID-19). Cell Commun Signal 20: 79, 2022.
23. Majidpoor J and Mortezaee K: Interleukin-6 in SARS-CoV-2 induced disease: Interactions and therapeutic applications. Biomed Pharmacother 145: 112419, 2022.
24. Zizzo G, Tamburello A, Castelnovo L, Laria A, Mumoli N, Faggioli PM, Stefani I and Mazzone A: Immunotherapy of COVID-19: Inside and beyond IL-6 signalling. Front Immunol 13: 795315, 2022.
25. Khan S, Shafiei MS, Longoria C, Schoggins JW, Savani RC and Zaki H: SARS-CoV-2 spike protein induces inflammation via TLR2-dependent activation of the NF-κB pathway. Elife 10: e68563, 2021.
26. Matsuyama T, Kubli SP, Yoshinaga SK, Pfeffer K and Mak TW: An aberrant STAT pathway is central to COVID-19. Cell Death Differ 27: 3209-3225, 2020.
27. Kaiser AE, Baniasadi M, Giansiracusa D, Giansiracusa M, Garcia M, Fryda Z, Wong TL and Bishayee A: Sulforaphane: A broccoli bioactive phytocompound with cancer preventive potential. Cancers (Basel) 13: 4796, 2021.
28. Barba FJ, Nikmaram N, Roohinejad S, Khelfa A, Zhu Z and Koubaa M: Bioavailability of glucosinolates and their breakdown products: Impact of processing. Front Nutr 3: 24, 2016.
29. Narbad A and Rossiter JT: Gut glucosinolate metabolism and isothiocyanate production. Mol Nutr Food Res 62: e1700991, 2018.
30. Lenzi M, Fimognari C and Hrelia P: Sulforaphane as a promising molecule for fighting cancer. Cancer Treat Res 159: 207-223, 2014.
31. Kubo E, Chhunchha B, Singh P, Sasaki H and Singh DP: Sulforaphane reactivates cellular antioxidant defense by inducing Nrf2/ARE/Prdx6 activity during aging and oxidative stress. Sci Rep 7: 14130, 2017.
32. Haristoy X, Angioi-Duprez K, Duprez A and Lozniewski A: Efficacy of sulforaphane in eradicating Helicobacter pylori in human gastric xenografts implanted in nude mice. Antimicrob Agents Chemother 47: 3982-3984, 2003.
33. Schepici G, Bramanti P and Mazzon E: Efficacy of sulforaphane in neurodegenerative diseases. Int J Mol Sci 21: 8637, 2020.
34. Li YP, Wang SL, Liu B, Tang L, Kuang RR, Wang XB, Zhao C, Song XD, Cao XM, Wu X, *et al*: Sulforaphane prevents rat cardiomyocytes from hypoxia/reoxygenation injury in vitro via activating SIRT1 and subsequently inhibiting ER stress. Acta Pharmacol Sin 37: 344-353, 2016.
35. Qi T, Xu F, Yan X, Li S and Li H: Sulforaphane exerts anti-inflammatory effects against lipopolysaccharide-induced acute lung injury in mice through the Nrf2/ARE pathway. Int J Mol Med 37: 182-188, 2016.
36. Folkard DL, Marlow G, Mithen RF and Ferguson LR: Effect of sulforaphane on NOD2 via NF-κB: Implications for Crohn's disease. J Inflamm (Lond) 12: 6, 2015.
37. Negi G, Kumar A and Sharma SS: Nrf2 and NF-κB modulation by sulforaphane counteracts multiple manifestations of diabetic neuropathy in rats and high glucose-induced changes. Curr Neurovasc Res 8: 294-304, 2011.
38. Xu C, Shen G, Chen C, Gélinas C and Kong ANT: Suppression of NF-kappaB and NF-kappaB-regulated gene expression by sulforaphane and PEITC through IkappaBalpha, IKK pathway in human prostate cancer PC-3 cells. Oncogene 24: 4486-4495, 2005.
39. Liu T, Zhang L, Joo D and Sun SC: NF-κB signaling in inflammation. Signal Transduct Target Ther 2: 17023, 2017.
40. Libermann TA and Baltimore D: Activation of interleukin-6 gene expression through the NF-kappa B transcription factor. Mol Cell Biol 10: 2327-2334, 1990.
41. McFarland BC, Hong SW, Rajbhandari R, Twitty GB Jr, Gray GK, Yu H, Benveniste EN and Nozell SE: NF-κB-induced IL-6 ensures STAT3 activation and tumor aggressiveness in glioblastoma. PLoS One 8: e78728, 2013.

42. Elliott CL, Allport VC, Loudon JA, Wu GD and Bennett PR: Nuclear factor-kappa B is essential for up-regulation of interleukin-8 expression in human amnion and cervical epithelial cells. Mol Hum Reprod 7: 787-790, 2001.
43. Fahey JW and Kensler TW: The challenges of designing and implementing clinical trials with broccoli sprouts… and turning evidence into public health action. Front Nutr 8: 648788, 2021.
44. Yagishita Y, Fahey JW, Dinkova-Kostova AT and Kensler TW: Broccoli or sulforaphane: Is it the source or dose that matters? Molecules 24: 3593, 2019.
45. Yagishita Y, Gatbonton-Schwager TN, McCallum ML and Kensler TW: Current landscape of NRF2 biomarkers in clinical trials. Antioxidants (Basel) 9: 716, 2020.
46. Zimmerman AW, Singh K, Connors SL, Liu H, Panjwani AA, Lee LC, Diggins E, Foley A, Melnyk S, Singh IN, *et al*: Randomized controlled trial of sulforaphane and metabolite discovery in children with autism spectrum disorder. Mol Autism 12: 38, 2021.
47. Gasparello J, D'Aversa E, Papi C, Gambari L, Grigolo B, Borgatti M, Finotti A and Gambari R: Sulforaphane inhibits the expression of interleukin-6 and interleukin-8 induced in bronchial epithelial IB3-1 cells by exposure to the SARS-CoV-2 spike protein. Phytomedicine 87: 153583, 2021.
48. Ordonez AA, Bullen CK, Villabona-Rueda AF, Thompson EA, Turner ML, Merino VF, Yan Y, Kim J, Davis SL, Komm O, *et al*: Sulforaphane exhibits antiviral activity against pandemic SARS-CoV-2 and seasonal HCoV-OC43 coronaviruses in vitro and in mice. Commun Biol 5: 242, 2022.
49. Bortolotti D, Gentili V, Rizzo S, Schiuma G, Beltrami S, Strazzabosco G, Fernandez M, Caccuri F, Caruso A and Rizzo R: TLR3 and TLR7 RNA sensor activation during SARS-CoV-2 infection. Microorganisms 9: 1820, 2021.
50. Papi C, Gasparello J, Zurlo M, Manicardi A, Corradini R, Cabrini G, Gambari R and Finotti A: Combined treatment of bronchial epithelial Calu-3 cells with peptide nucleic acids targeting miR-145-5p and miR-101-3p: Synergistic enhancement of the expression of the cystic fibrosis transmembrane conductance regulator (CFTR) gene. Int J Mol Sci 23: 9348, 2022.
51. Gasparello J, Papi C, Zurlo M, Gambari L, Rozzi A, Manicardi A, Corradini R, Gambari R and Finotti A: Treatment of human glioblastoma U251 cells with sulforaphane and a peptide nucleic acid (PNA) targeting miR-15b-5p: Synergistic effects on induction of apoptosis. Molecules 27: 1299, 2022.
52. Heiss E, Herhaus C, Klimo K, Bartsch H and Gerhäuser C: Nuclear factor kappa B is a molecular target for sulforaphane-mediated anti-inflammatory mechanisms. J Biol Chem 276: 32008-32015, 2001.
53. Caruso A, Caccuri F, Bugatti A, Zani A, Vanoni M, Bonfanti P, Cazzaniga ME, Perno CF, Messa C and Alberghina L: Methotrexate inhibits SARS-CoV-2 virus replication 'in vitro'. J Med Virol 93: 1780-1785, 2021.
54. Livak KJ and Schmittgen TD: Analysis of relative gene expression data using real-time quantitative PCR and the 2(-Delta Delta C(T)) method. Methods 25: 402-408, 2001.
55. Van Der Spoel D, Lindahl E, Hess B, Groenhof G, Mark AE and Berendsen HJC: GROMACS: Fast, flexible, and free. Comput Chem 26: 1701-1718, 2005.
56. Pronk S, Páll S, Schulz R, Larsson P, Bjelkmar P, Apostolov R, Shirts MR, Smith JC, Kasson PM, van der Spoel D, *et al*: GROMACS 4.5: A high-throughput and highly parallel open source molecular simulation toolkit. Bioinformatics 29: 845-854, 2013.
57. Marrink SJ, Risselada HJ, Yefimov S, Tieleman DP and de Vries AH: The MARTINI force field: Coarse grained model for biomolecular simulations. J Phys Chem B 111: 7812-7824, 2007.
58. Bereau T and Kremer K: Automated parametrization of the coarse-grained Martini force field for small organic molecules. J Chem Theory Comput 11: 2783-2791, 2015.
59. Lamprakis C, Andreadelis I, Manchester J, Velez-Vega C, Duca JS and Cournia Z: Evaluating the efficiency of the Martini force field to study protein dimerization in aqueous and membrane environments. J Chem Theory Comput 17: 3088-3102, 2021.
60. Souza PCT, Thallmair S, Conflitti P, Ramírez-Palacios C, Alessandri R, Raniolo S, Limongelli V and Marrink SJ: Protein-ligand binding with the coarse-grained Martini model. Nat Commun 11: 3714, 2020.
61. Honorato RV, Roel-Touris J and Bonvin AMJJ: MARTINI-based protein-DNA coarse-grained HADDOCKing. Front Mol Biosci 6: 102, 2019.
62. Periole X, Cavalli M, Marrink SJ and Ceruso MA: Combining an elastic network with a coarse-grained molecular force field: Structure, dynamics, and intermolecular recognition. J Chem Theory Comput 5: 2531-2543, 2009.
63. Zhang X, Wu K, Wang D, Yue X, Song D, Zhu Y and Wu J: Nucleocapsid protein of SARS-CoV activates interleukin-6 expression through cellular transcription factor NF-kappaB. Virology 365: 324-335, 2007.
64. du Preez HN, Aldous C, Kruger HG and Johnson L: N-Acetylcysteine and other sulfur-donors as a preventative and adjunct therapy for COVID-19. Adv Pharmacol Pharm Sci 2022: 4555490, 2022.
65. Zinovkin RA and Grebenchikov OA: Transcription factor Nrf2 as a potential therapeutic target for prevention of cytokine storm in COVID-19 patients. Biochemistry (Mosc) 85: 833-837, 2020.
66. Cuadrado A, Pajares M, Benito C, Jiménez-Villegas J, Escoll M, Fernández-Ginés R, Garcia Yagüe AJ, Lastra D, Manda G, Rojo AI and Dinkova-Kostova AT: Can activation of NRF2 Be a strategy against COVID-19? Trends Pharmacol Sci 41: 598-610, 2020.
67. Kow CS, Ramachandram DS and Hasan SS: Use of sulforaphane in COVID-19: Clinical trials are needed. Mol Immunol 145: 78-79, 2022.